

Design of Mott and topological phases on buckled 3d-oxide honeycomb lattices

David Doennig,¹ Santu Baidya,² Warren E. Pickett,³ and Rossitza Pentcheva^{2,1,*}

¹*Forschungs-Neutronenquelle Heinz Maier-Leibnitz (FRM II),*

Technische Universität München, Lichtenbergstraße 1, 85748 Garching, Germany

²*Department of Physics and Center for Nanointegration Duisburg-Essen (CENIDE),*

University of Duisburg-Essen, Lotharstr. 1, 47057 Duisburg, Germany

³*Department of Physics, University of California Davis, One Shields Avenue, Davis, CA 95616, U.S.A.*

(Dated: November 2, 2015)

Perovskite bilayers with (111)-orientation combine a honeycomb lattice as a key feature with the strongly correlated, multiorbital nature of electrons in transition metal oxides. In a systematic DFT+ U study of (111)-oriented $(\text{LaXO}_3)_2/(\text{LaAlO}_3)_4$ superlattices, we establish trends in the evolution of ground states versus band filling in (111)-oriented $(\text{LaXO}_3)_2/(\text{LaAlO}_3)_4$ superlattices, with X spanning the entire 3d transition metal series. The competition between local quasi-cubic and global triangular symmetry triggers unanticipated broken symmetry phases, with mechanisms ranging from Jahn-Teller distortions, to charge-, spin-, and orbital-ordering. LaMnO_3 , where spin-orbit coupling opens a sizable gap in the Dirac-point Fermi surface, emerges as a topological Chern insulator.

PACS numbers: 73.21.Fg, 73.22.Gk, 75.70.Cn

INTRODUCTION

Synthesis and characterization of atomically abrupt transition metal oxide (TMO) heterostructures have revealed a broad platform of unanticipated functionalities with potential to enhance next generation electronics and spintronics capabilities by controlling charge, spin, orbital, and lattice degrees of freedom at the nanoscale.[1, 2]

The earlier focus on perovskite materials with the (001) growth orientation - prominent examples here being e.g. the interface between LaAlO_3 and SrTiO_3 (LAO/STO)[3, 4] or nickelate superlattices [5] - has recently been extended to the (111) orientation.[6, 7] In the latter, two triangular BO_6 sublattices form a buckled honeycomb lattice, topologically equivalent to graphene. The honeycomb lattice itself introduces exotic possibilities: considering an alternating, next nearest neighbor (nnn) *imaginary* hopping amplitude, Haldane obtained a quantum spin Hall (QSH) system without explicit external field.[8] In the Kane-Mele elucidation[9] of the honeycomb lattice, topological behavior originated from spin-orbit coupling (SOC) entanglement of band character. Later, Raghu *et al.*[10] proposed that topological character can be generated by strong interactions (even in the mean field approximation). Wright generalized Haldane's model to a *buckled honeycomb lattice* in which magnetic flux, alternating in orientation in neighboring cells, leads to a Chern (quantum anomalous Hall [QAH]) insulator[11] with topologically protected gapless edge states. These specific models are, however, challenging to realize in real materials, and viable Chern insulators remain to be realized.

Compared to graphene and common topological insulators (TI), TMOs possess not only larger band gaps,

but offer an enormously richer palette of possibilities due to several distinctive features: correlated electron behavior causing spin, charge, and orbital instabilities, multi-orbital configurations combined with relativistic effects, viz. spin-orbit coupling (SOC). Below we demonstrate that the interplay of strong interactions and SOC effects produce specific spin-fermion systems as candidates for QSH or QAH systems in the 3d (111) bilayers with buckled honeycomb lattice.

The idea of constructing a (111) bilayer from perovskite TMO was introduced by Xiao *et al.* for 4d and 5d systems, pointing to possibilities for “interface engineering of quantum anomalous Hall effects”. [12] Building on this foundation, Yang *et al.*[13] and Rüegg and Fiete[14] applied a tight-binding (TB) model for $(\text{LaNiO}_3)_2/\text{LAO}$, and demonstrated that in certain ranges of parameters and magnetic order topological insulating phases can result from ordering of a complex combination of e_g orbitals.[14]

Complementary to tight-binding models, material-specific density functional theory (DFT) can both contribute towards a fundamental understanding as well as guide the search for actual materials realizations. Besides examples for 5d systems[15], DFT studies including strong local interaction effects (see below) have recently predicted a Dirac-point Fermi surface for $\text{STO}(111)$ [16] and $\text{LNO}(111)$ bilayers, quantum confined within LAO.[13, 14, 17] In these cases the Dirac point is ‘protected’ by symmetry; sublattice symmetry breaking leads to gap-opening charge-disproportionated states.[16, 17]

To identify further promising systems as well as to elucidate the underlying *design principles* of functionalities, we have explored systematically the effect of band filling on the electronic ground state in (111)-oriented $(\text{LaXO}_3)_2/(\text{LaAlO}_3)_4$ superlattices, where X spans the

range of trivalent $3d$ ions Ti-Cu. Despite the fact that these systems, unlike LAO/STO(111), have nonpolar interfaces - i.e. there is no valence mismatch across the interface, so all transition metal cations retain X^{3+} configurations - unexpected phases proliferate. Competition between local pseudocubic symmetry and global trigonal symmetry as well as additional flexibility, provided by the magnetic and spin degrees of freedom of $3d$ ions, lead to a broad array of distinctive broken symmetry ground states, offering a platform to design 2D electronic functionalities.

Moreover, while Chern insulators have so far been sought mainly in magnetically doped TIs[18], or very recently, by combining trivial magnetic insulators with a material with large SOC, either in double perovskites[19] or rock-salt compounds[20, 21], two of our systems display simultaneous time reversal symmetry breaking and SOC-driven gap opening. These are first examples in a solely $3d$ system with gap sizes large enough to support room-temperature applications.

DFT calculations were performed on (111)-oriented $(\text{LaXO}_3)_2/(\text{LaAlO}_3)_4$ superlattices with $X = 3d$, using the all-electron full-potential linearized augmented-plane-wave (LAPW) method, as implemented in the WIEN2k code [22]. For the exchange-correlation functional we used the generalized gradient approximation (GGA) [23]. Static local electronic correlations were included in the GGA+ U approach [24] with $U = 5\text{ eV}$, $J = 0.7\text{ eV}$ (for all $X = \text{Ti-Cu } 3d$) and $U = 8\text{ eV}$ (La 4f). Systematic investigations of the influence of U show that the results are robust with respect to variation of the U parameter in a reasonable range of values. Additional calculations with the modified Becke-Johnson [25] potential support the obtained electronic behavior.

The lateral lattice constant is fixed to $a_{\text{LAO}} = 3.79\text{ \AA}$, corresponding to superlattices grown on a LAO(111) substrate, unless otherwise stated. Octahedral tilts and distortions were fully taken into account when relaxing atomic positions, whether constrained to P321 symmetry or fully released to P1 symmetry. Additionally, the out-of-plane lattice parameter c was optimized for all superlattices. Spin-orbit coupling (SOC) was treated using the second-variational method. AHC was calculated using wannier90[26, 27] interfaced with Wien2k[28].

Trends across the $3d$ series: A central aspect in the $(\text{LaXO}_3)_2/(\text{LaAlO}_3)_4$ (111) honeycomb bilayers is their strong deviation from their bulk analogs. Certain recurring features tied to the t_{2g} and e_g distinction can be identified, thus we discuss them separately.

t_{2g} systems: For the t_{2g} subshell the dominating feature is a competition between local pseudo-cubic symmetry and the underlying threefold+inversion symmetry (“P321”) of the ideal bilayer. The (111) bilayering reduces the octahedral symmetry to trigonal and splits the t_{2g} orbital triplet into $a_{1g} + e'_g$, with the former having zero angular momentum around the \hat{c} bilayer axis

while the latter orbital doublet forms a representation for $m_\ell = \pm 1$ angular momentum. Breaking this symmetry allows occupation of the cubic d_{xy} , d_{yz} , or d_{xz} orbitals.

$X = \text{Ti}^{3+} 3d^1$. The above scenario arises most vividly for the LaTiO_3 bilayer, which displays the richest behavior among the t_{2g} systems. The ground state at the lateral lattice constant of LaAlO_3 (a_{LAO}), pictured in Fig. 1a), is a ferromagnetic (FM) orbitally ordered Mott insulator, displaying staggered d_{xz} , d_{yz} occupation and a very narrow (0.2 eV bandwidth) lower Hubbard band. This is in contrast to bulk LaTiO_3 which is a distorted $Pbnm$, G-type antiferromagnetic (AFM) Mott insulator with $1/\sqrt{3}(d_{xy} + d_{yz} + d_{zx})$ orbital order [29, 30]. Consistent with this extremely localized character, the corresponding AFM state with the same orbital polarization, shown in Fig. 1e, is only 4 meV/u.c. higher in energy, suggesting a weak exchange coupling of ~ 1 meV.

Constraining the symmetry to P321, thereby keeping the two Ti ions related by symmetry, results in e'_g orbital polarization with bands touching at K and K' (Fig. 1f). This degeneracy protects the system against the Mott insulating gap, presenting a special case of strong correlation effects being rendered ineffectual by an imposed symmetry. Despite its high energy cost (0.4 eV/Ti), this state is intriguing due to the unusual direction reversal of bands in the vicinity of K and K' points (note zoom-in of the band structure in Fig. 1g). This intertwining of bands suggests topological character.

Inclusion of SOC with out-of-plane magnetization leads to a band inversion and a resulting gap (green line in Fig. 1g) and a nonzero anomalous Hall conductivity (AHC). The disparity at K and K' signals the loss of equivalence of the two Ti ions, reflected in an surprisingly large orbital moment of one of the ions: $0.11\mu_B$ versus just $0.01\mu_B$ on the other.

Ti orbital polarization is highly susceptible to strain-tuning: applying tensile strain by imposing the lateral lattice constant of SrTiO_3 tips the pseudo-cubic/trigonal symmetry balance, stabilizing occupation of the a_{1g} orbital (Fig. 1h). The band structure just below the gap is comprised of two filled bands with Dirac crossings at K and K', similar to the analogous LAO/STO(111) case,[17] where the $3d^{0.5}$ band filling fixes the Dirac points at E_F instead.

$X = \text{V}^{3+} 3d^2$. The AFM ground state of the LaVO_3 -bilayer, displayed in Fig. 1b, is gapped due to occupation of the majority e'_g doublet. This is insensitive to strain and at variance with the bulk G-type d_{xz} , d_{yz} orbital ordering (d_{xy} is occupied on all sites)[30, 31]. Thus in this LaVO_3 bilayer trigonal symmetry splitting dominates over the pseudocubic crystal field. The FM state (Fig. 1c) with the same orbital polarization is 73 meV/u.c. higher in energy, and has four bands topologically similar to those of the metastable 2LaTiO_3 case (Fig. 1f), with the difference that now the entire set of bands is filled.

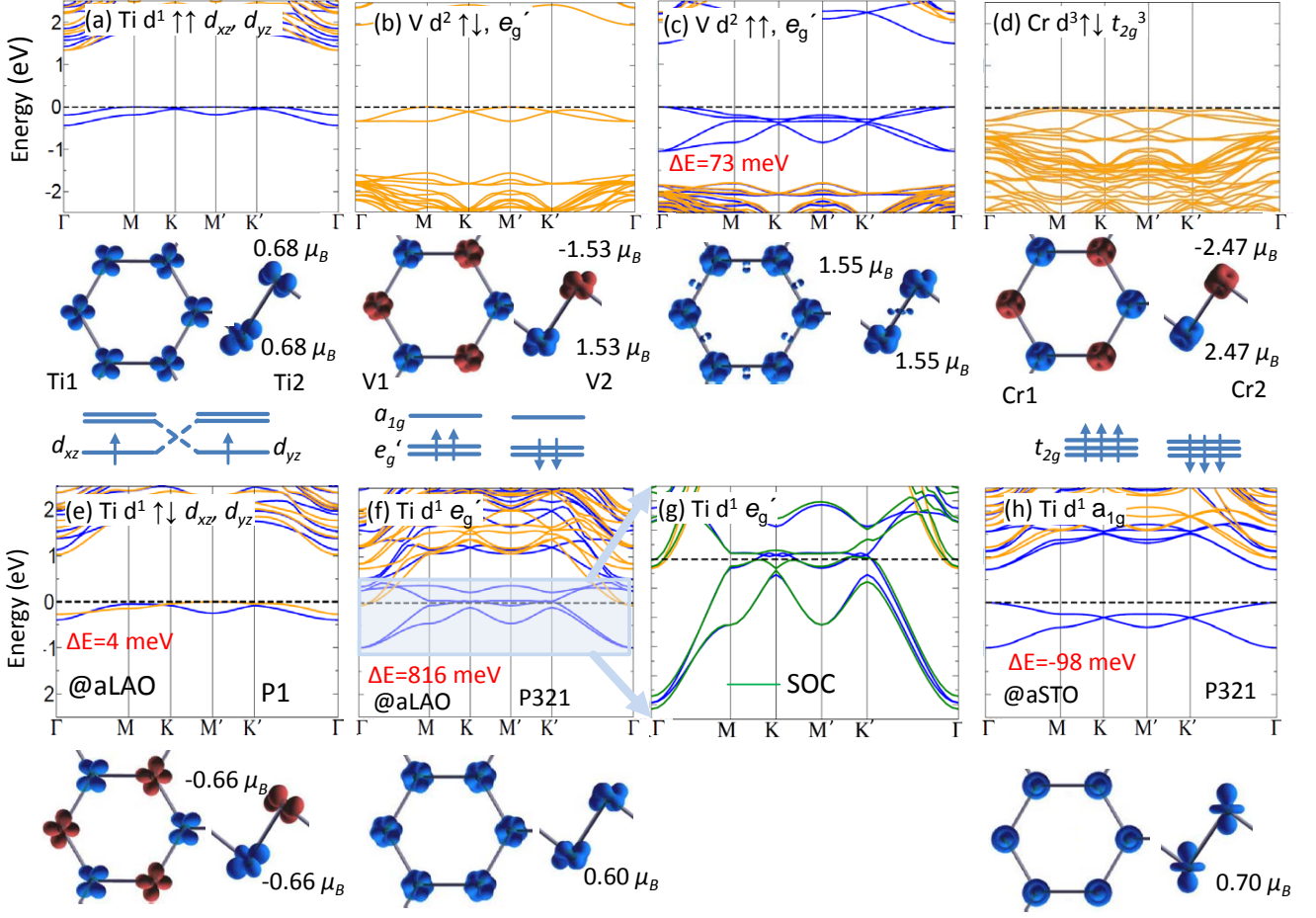


FIG. 1: Electronic ground (a-d) and selected metastable (e-h) states in $(\text{LaXO}_3)_2/(\text{LaAlO}_3)_4(111)$ for t_{2g} systems $X=\text{Ti}, \text{V}, \text{Cr}$. Shown are the band structures with blue/orange denoting the majority/minority bands, and isosurfaces of the spin density, with majority in blue and minority in red. In cases (a,e,h) the integration range is $E_F-1\text{eV}, E_F$ to emphasize the orbital polarization. Energies of metastable states are provided in red.

$X=\text{Cr}^{3+} 3d^3$. The Cr bilayer is electronically trivial: a half-filled t_{2g} -band ($t_{2g,\uparrow}^3, S=\frac{3}{2}$), thus no orbital degrees of freedom, and antiferromagnetic order (Fig. 1d).

e_g systems: Now we turn to the e_g systems. Consistent with the tight-binding model of Xiao *et al.*[12] a distinctive set of four bands emerges for ferromagnetic coupling with an open e_g subshell: nearly flat bottom and top bands interconnected by two dispersive bands, providing a Dirac point crossing at the K and K' points and quadratic contact with the flat bands at the Γ point (cf. Fig. 2a-c,h,l). A key finding is that a pinning of the Dirac point at E_F is not solely determined by band filling, but also by an interplay of orbital and spin degrees of freedom, as proven for the cases of $X=\text{Mn}, \text{Co}$ and Ni. Equivalence of the two sublattices again becomes crucial. This symmetry is found to be broken in *all* e_g system ground states where the Dirac point is initially at the Fermi level. We identify distinct origins of symmetry

breaking and the resulting gap opening in each system, as discussed below.

$X=\text{Mn}^{3+} 3d^4$. The LaMnO_3 bilayer renders one of the promising cases where, within P321 symmetry, the system exhibits a Dirac point Fermi surface within the e_g bands (Fig.2a). The high-spin (HS) Mn ion ($t_{2g,\uparrow}^3 e_{g,\uparrow}^1$ with the majority e_g -band half-filled putting the Dirac point at E_F) is unstable to Jahn-Teller distortion. Releasing structural symmetry restrictions leads to an elongation of the apical Mn-O bond lengths to 2.07-2.11 Å and variation of the basal distances between 1.89-1.98 Å, associated with alternating $d_{3y^2-r^2}, d_{3x^2-r^2}$ occupation on the A and B sublattices (Fig. 2e). This symmetry breaking opens a gap of 0.8 eV and also lifts the quadratic band touching degeneracy at Γ . The Jahn-Teller distortion is also present in the AFM order (Fig. 2i), which is 88 meV/u.c. higher in energy. The significantly flatter bands reflect electronic decoupling of the two sublattices,

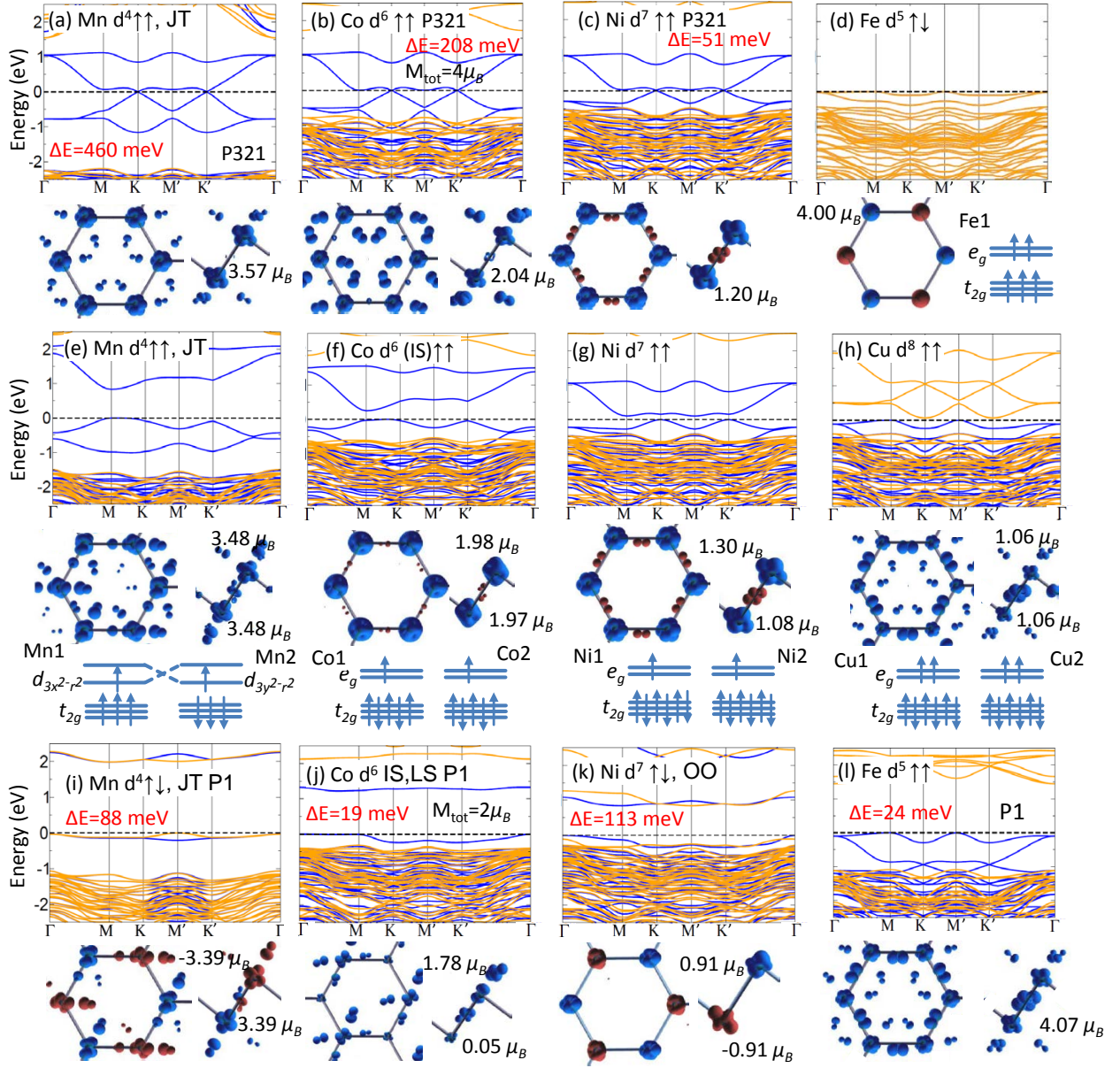


FIG. 2: Presentation as in Fig. 1, but for e_g systems $X=\text{Mn, Fe, Co, Ni, and Cu}$. A striking feature is the similarity in band structure of $X=\text{Mn, Co, Ni}$, despite the formally different band filling: a Dirac point Fermi surface within P321 (a)-(c) and a gap opening due to symmetry breaking. The ground state results are presented in (d)-(h).

similar to the AFM LaNiO_3 bilayer (Fig. 2k), discussed below.

$X=\text{Fe}^{3+} 3d^5$. The ground state of the LaFeO_3 bilayer is a HS AFM band insulator with nearly spherically symmetric charge and spin density on the Fe site, characteristic of a half-filled $3d$ band ($t_{2g}^3 e_g^2$ with $S=\frac{5}{2}$, cf. Fig 2d). For comparison, bulk LaFeO_3 is a G-type AFM with orthorhombic $Pnma$ structure. The metastable FM configuration exhibits the previously discussed set of four bands, albeit now these are fully occupied for the majority spin channel (cf. Fig 2l).

$X=\text{Co}^{3+} 3d^6$. Bulk LaCoO_3 has a low spin (LS) (t_{2g}^6)

narrow gap insulating ground state, but becomes ferromagnetic e.g. as a strained film [32]. A rich set of (metastable) states with respect to spin degrees of freedom can be anticipated and is indeed realized in the LaCoO_3 bilayer. Constraining symmetry to P321 renders another case where the Fermi level is pinned at a Dirac point (Fig. 2b). This state lies 0.21 eV above the broken symmetry ground state of FM intermediate spin (IS) ($t_{2g}^5 e_g^1$) insulator with a moment of $1.97\mu_B$ (Fig. 2f). Orbital ordering of the e_g electron and t_{2g} hole drives the breaking of symmetry, analogous to the case of Mn but with a smaller band gap.

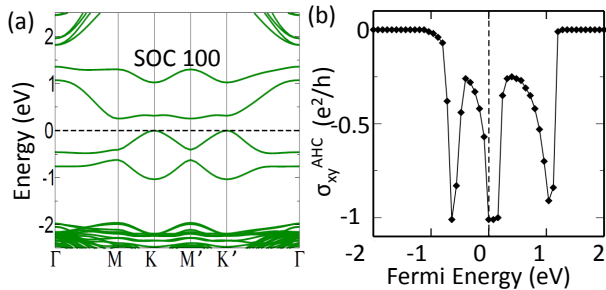


FIG. 3: Effect of SOC on $(\text{LaMnO}_3)_2/(\text{LaAlO}_3)_4$ a) band structure for magnetization along $[100]$; b) calculated AHC for a range of Fermi levels, plotted in units of (e^2/h) , shows a Chern number of unity.

A further metastable state, only 19 meV less favorable, exhibits a new type of *spin state symmetry breaking* in which the two Co sublattices assume IS and LS states with very flat bands accompanied by (and presumably caused by) a $d_{x^2-y^2}$ orbital occupation on the IS Co sublattice (Fig. 2j).

$X=\text{Ni}^{3+} 3d^7$. Bulk LaNiO_3 is a $R\bar{3}c$ correlated metal. [29]. Within P321 symmetry a Dirac-point Fermi surface is obtained for the LaNiO_3 bilayer (cf. Fig. 2c), as previously reported [13, 14, 17]. However, breaking the equivalency of the two triangular sublattices opens a gap of 0.25 eV at the Fermi level (cf. Fig. 2g)[17]. Here the mechanism is disproportionation of the Ni sublattice, expressed in different magnetic moments of 1.30 and 1.08 μ_B . AFM coupling of the two bilayers results in flat bands (Fig. 2k), defining a band gap of ~ 1 eV with orbital polarization at the Ni sites, as recently observed in a NdNiO_3 bilayer.[6] This illustrates how antiferromagnetic order provides the necessary decoupling of the two trigonal bilayers, analogous to the $\text{La}_2\text{NiAlO}_6$ double perovskite where the single triangular Ni-layers are separated by Al-layers [17].

$X=\text{Cu}^{3+} 3d^8$. This case yields a straightforward $e_{g,\uparrow}^2$ $S=1$ ion at half filling of the e_g bands, with large optical (spin-conserving) gap but with very low energy spin-flip excitations (Fig. 2h, see also [12]). Although Cu^{3+} is uncommon (bulk LaCuO_3 is metallic and must be synthesized under pressure),[33] it might be stabilized by non-equilibrium epitaxial synthesis.

Despite the formal difference in band filling for $X=\text{Mn}$, Co, and Ni, an unexpected analogy occurs in the electronic structure of these bilayers: a Dirac-point Fermi surface when constrained to P321 symmetry reverts to a gapped Mott insulator state, being driven by symmetry breaking of distinct origin: a Jahn-Teller distortion in LaMnO_3 ; a spin transition to IS accompanied by orbital order in LaCoO_3 ; and a charge disproportionation in LaNiO_3 .

Spin-orbit coupling. Generally, no significant SOC is

expected in the $3d$ series beyond minor band splittings and small magnetocrystalline anisotropy. However, an unusually strong effect arises in LaMnO_3 and LaCoO_3 : SOC gaps both the Dirac points at K and K' as well as the quadratic band touching at Γ . $(\text{LaMnO}_3)_2$ shows a stronger influence of SOC, with an in-plane $[100]$ easy axis (Fig. 3a), while $(\text{LaCoO}_3)_2$ has an out-of plane easy axis. The anomalous Hall conductivity[26–28] plotted versus (rigid band) chemical potential in (Fig. 3b), determines $(\text{LaMnO}_3)_2$ as a $C=-1$ Chern insulator. The gap of 200 meV indicates the possibility of room temperature applications.

Apart from three cases of filled subshells that stabilize symmetric phases, the buckled $3d$ honeycomb bilayers encounter and succumb to a variety of symmetry-breaking forces: (1) orbital ordering including competition between occupation of real pseudocubic orbitals (d_{xy} , d_{xz} , d_{yz} for t_{2g} ; $d_{x^2-y^2}$ and d_{z^2} for e_g) and their triangular lattice counterparts; (2) charge disproportionation, (3) spin-state differentiation, and (4) Jahn-Teller distortion.

Spin-orbit coupling, typically important rather in $4d$ and $5d$ than $3d$ systems, is found to gap the Dirac point Fermi surface, in two members of this series $X=\text{Mn}$ and Co, inducing Chern insulating phases with gap size (for LaMnO_3) allowing consideration for room temperature applications.

This study outlines the variety of possibilities for unusual ground states and topological behavior in this “ $3d$ palette” of two-dimensional oxide honeycomb lattices. The predicted trends should stimulate research on the experimental realization of these phases, which can be combined into numerous hybrid systems using multilayer growth techniques. Doping of these materials will provide further possibilities to tune functionalities, interesting for basic research reasons as well as for potential applications.

Discussions with Binghai Yan are gratefully acknowledged. This work was partially supported by the German Science Foundation within SFB/TR80, project G3 (to R.P. and D.D.) and by U.S. Department of Energy Grant No. DE-FG02-04ER46111 (to W.E.P.).

* Electronic address: Rossitza.Pentcheva@uni-due.de

- [1] H. Y. Hwang, Y. Iwasa, M. Kawasaki, B. Keimer, N. Nagaosa and Y. Tokura, Nat. Mater. **11**, 103 (2012).
- [2] J. Mannhart, and D. G. Schlom, Science **327**, 1607 (2010).
- [3] R. Pentcheva, and W. E. Pickett, J. Phys.: Condens. Matter **32**, 043001 (2010).
- [4] P. Zubko, S. Gariglio, M. Gabay, P. Ghosez, and J.-M. Triscone, Annu. Rev. Condens. Matter Phys. **2**, 141 (2011).
- [5] J. Chaloupka, and G. Khaliullin, Phys. Rev. Lett. **100**, 016404 (2008).

- [6] S. Middey, D. Meyers, M. Kareev, E. J. Moon, B. A. Gray, X. Liu, J. W. Freeland and J. Chakhalian, *Appl. Phys. Lett.* **101**, 261602 (2012).
- [7] M. Gibert, P. Zubko, R. Scherwitzl, J.-M. Triscone, *Nat. Mater.* **11**, 195 (2012).
- [8] F. D. M. Haldane, *Phys. Rev. Lett.* **61**, 2015 (1988).
- [9] C. Kane and E. Mele, *Phys. Rev. Lett.* **95**, 226801 (2005).
- [10] S. Raghu, X. L. Qi, C. Honerkamp, and S.-C. Zhang, *Phys. Rev. Lett.* **100**, 156401 (2008).
- [11] A. R. Wright, *Sci. Rep.* **3**, 2736 (2013).
- [12] D. Xiao, W. Zhu, Y. Ran, N. Nagaosa and S. Okamoto, *Nature Commun.* **2**, 596 (2011).
- [13] K.-Y. Yang, W. Zhu, D. Xiao, S. Okamoto, Z. Wang, and Y. Ran, *Phys. Rev. B* **84**, 201104(R) (2011).
- [14] A. Rüegg, and G. A. Fiete, *Phys. Rev. B* **85**, 245131 (2011).
- [15] J. L. Lado, V. Pardo, and D. Baldomir, *Phys. Rev. B* **88**, 155119 (2013).
- [16] D. Doennig, W. E. Pickett and R. Pentcheva, *Phys. Rev. Lett.* **111**, 126804 (2013).
- [17] D. Doennig, W. E. Pickett, and R. Pentcheva, *Phys. Rev. B* **89**, 121110 (2014).
- [18] C.-Z. Chang, *et al.*, *Science* **340**, 167 (2013).
- [19] A. M. Cook, A. Paramekanti, *Phys. Rev. Lett.* **113**, 077203 (2014).
- [20] K. F. Garrity and D. Vanderbilt, *Phys. Rev. B* **90**, 121103(R) (2014).
- [21] H. Zhang, J. Wang, G. Xu, Y. Xu and S.-C. Zhang, *Phys. Rev. Lett.* **112**, 096804 (2014).
- [22] P. Blaha, K. Schwarz, G. K. H. Madsen, D. Kvasnicka, and J. Luitz, *WIEN2k, An Augmented Plane Wave Plus Local Orbitals Program for Calculating Crystal Properties*, ISBN 3-9501031-1-2 (Vienna University of Technology, Vienna, Austria, 2001).
- [23] J. P. Perdew, K. Burke and M. Ernzerhof, *Phys. Rev. Lett.* **77**, 3865 (1996).
- [24] V. I. Anisimov, J. Zaanen, and O. K. Andersen, *Phys. Rev. B* **44**, 943 (1991).
- [25] F. Tran and P. Blaha, *Phys. Rev. Lett.* **102**, 226401 (2009).
- [26] A. A. Mostofi, J. R. Yates, Y. S. Lee, I. Souza, I. Vanderbilt, N. Marzari, *Comput. Phys. Commun.* **178**, 685 (2008).
- [27] X. Wang, J. R. Yates, I. Souza, I. Vanderbilt, *Phys. Rev. B* **74**, 195118 (2006).
- [28] J. Kuneš, R. Arita, P. Wissgott, A. Toschi, H. Ikeda, K. Held, *Comp. Phys. Commun.* **181**, 1888 (2010).
- [29] T. Arima, Y. Tokura and J. B. Torrance, *Phys. Rev. B* **48**, 17006 (1993).
- [30] E. Pavarini, S. Biermann, A. Poteryaev, A. I. Lichtenstein, A. Georges, and O. K. Andersen, *Phys. Rev. Lett.* **92**, 176403 (2004).
- [31] M. De Raychaudhury, E. Pavarini, O.K. Andersen, *Phys. Rev. Lett.* **99**, 126402 (2007).
- [32] H. Hsu, P. Blaha and R. M. Wentzcovitch, *Phys. Rev. B* **85**, 140404 (2012).
- [33] M. Karppinen, H. Yamauchi, T. Ito, H. Suematsu, O. Fukunaga, *Matl. Sci. & Eng.* **41**, 59 (1996).